1999-01-5622

Supersonic Business Jet Design Through Bi-Level Integrated System Synthesis

Jeremy S. Agte
United States Air Force

Jaroslaw Sobieszczanski-Sobieski
NASA Langley Research Center

Robert R. Sandusky, Jr.
George Washington Univ.

ABSTRACT

New optimization methods that are intended as an improvement over traditional design methodology often require the design model itself to be developed in a non-traditional manner. This paper describes the tailoring of a supersonic business jet design model to the Bi-Level Integrated System Synthesis (BLISS) optimization method. Included is a brief discussion of BLISS, the development and implementation of the design model, application of the design constraints, and a survey of favorable results. For discussion purposes, the design model is 'tailored' to the optimization method, not vice versa, to illustrate the model's unique development.

INTRODUCTION

Until the latter part of the 20th Century, the design of engineering systems was mostly unaided by the large data processing benefits of computers. While this limitation did not prevent design through methodical procedure, it did lead to the development of traditional design methodologies that are less than optimal for complete computer implementation. For instance, modern aircraft design, especially in the preliminary stages, relies heavily upon knowledge and data derived from past design endeavors. Historical trends in this data are often collected in tabular or plot form and used to derive such values as weight estimations, drag counts, or even some stability characteristics. These are not bad practices, indeed they are often the cheapest and most effective means of aircraft design, provided the resources of the near past. However, as the transition is made from a computer free design environment to one in which computers perform nearly all of the data processing and computational work at even the conceptual stage, new processes are developed in order to take full advantage of modern computing abilities. Several Multidisciplinary Design Optimization (MDO) methods, to date, attempt to meet this challenge (survey papers: Balling and Sobieszczanski-Sobieski, 1996; and Sobiesczcanski-Sobieski, J., and Haftka, R. T. 1997). An often overlooked point, however, is that while the computational process changes with technology, the manner in which the design model is tailored to that process must evolve as well. Certain requirements of the process will guide this evolution.

For example, computer implementation of the above MDO methods requires that the mathematical model of a tailored system properly represent trade-offs and constraints influencing the particular design optimization objective. Consider the weight-drag trade-off in a wing design as an illustration of this. It occurs by virtue of a redistribution of the wing structural stiffness to allow an inboard shift of the lift resultant. This reduces the bending moment and, accounting for stress and buckling constraints, lightens the structure. However, in maintaining the same magnitude of lift, wing and trim drag components increase. The equation for an objective function of range would then have the resulting weight and drag influences opposing each other throughout the optimization. Also important is the correct formulation of constraints in this execution. Stress and buckling constraints must be completely correct to ensure the proper trade-off relationship, and additional constraints may be necessary to account for any assumptions or approximations made in the development of the model.

A second requirement, if the particular MDO method is gradient-guided as in the case of BLISS, is that data flow between and across optimization levels must be continuous throughout method execution. For example, propulsion data for a given aircraft engine must be available as a continuous function of Mach number and altitude, rather than in the tabular form of an engine deck. Additionally, the computational calculation of derivatives necessary for optimization routines is simplified significantly

when the internal mechanisms of each module are continuous functions. This means that it is often beneficial to return to fundamental equations, while traditional aircraft design methodology might rely more heavily upon historical trends and experimental data in the form of nomograms.

The model described herein is one example of how these considerations are accounted for in the tailoring of a business jet design to an MDO method.

OPTIMIZATION METHOD

Bi-Level Integrated System Synthesis (BLISS), currently under development at NASA's Langley Research Center (survey Sobieszczanski-Sobieski, Agte, and Sandusky, 1998, for complete details), is the method for which the business jet design model is tailored. BLISS is a method for optimization of engineering systems that separates the system level optimization from potentially numerous autonomous subsystem optimizations. As shown in Figure 1, it utilizes a system architecture in which design and behavior variables are split into three categories. X-variables are those design variables optimized at the local level and are unique to each particular subsystem. Behavior variables that are output from one subsystem and input to another are designated Y, and the system level design variables are specified as Z. System level variables are those shared by at least two subsystems.

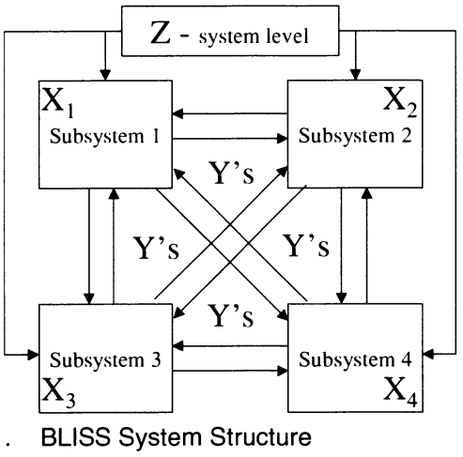

Figure 1. BLISS System Structure

The first step in the BLISS optimization occurs at the subsystem level. Here, Z-variables are frozen and an improvement in the objective function is sought after in the local variable subdomains. The second step achieves improvement through the system level variables and is linked to the first step by optimum sensitivity data. These steps alternate until convergence. A flowchart of the method is shown in Figure 2.

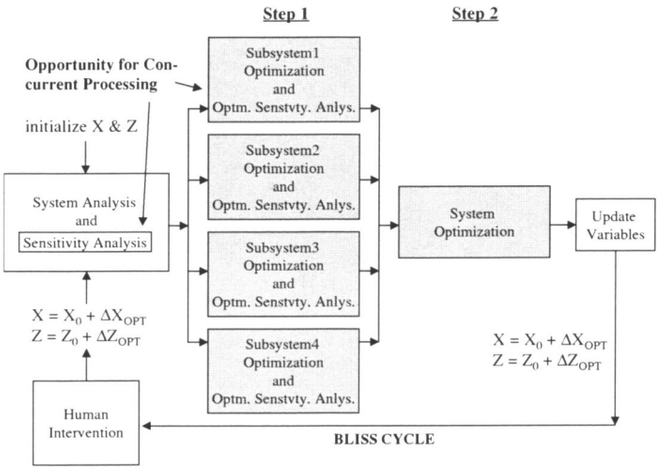

Figure 2. BLISS Cycle

Note that the output of step 1 is an optimum change in the local design variables, ΔX_{OPT}, in the presence of constant Z, and the output of step 2 is an optimum change in system design variables, ΔZ_{OPT}.

MODEL DEVELOPMENT

Requirements and constraints for the supersonic business jet come from the 1995/96 AIAA Student Aircraft Design Competition. Applying the BLISS method to this design problem necessitates the division of the aircraft system into several subsystems. These include structures, aerodynamics, propulsion, and range modules. The structures module consists of a wingbox divided into several bays along the half-span, modeled by an elaborate skin-stringer approximation. Aerodynamics includes the calculation of lift and drag through several fundamental equations applied independently to each of the aircraft's lifting surfaces. Finally, the propulsion module is composed of a surface fit to engine deck data, and the range module uses the Breguet range equation to construct the overall system objective function.

STRUCTURES – The structures module consists of a skin-stringer representation of the internal wingbox bays, the output of which is used to compute wing weight. Weights of several other aircraft components are determined through the use of statistical regression-analysis equations. To represent the trade-off between structural weight and aerodynamic drag, the analysis accounts for wing twist due to torsion and due to bending in the presence of a sweep angle, while satisfying stress and local skin buckling constraints.

A three bay wingbox constitutes the structural wing model. Ribs separating the bays are perpendicular to the leading edge at the root chord and at one-third and two-thirds of the half-span. This configuration is depicted in Figure 3, with the bays numbered accordingly. Their length and height are allowed to change as taper ratio, wing sweep, thickness-to-chord ratio, wing span, and aspect ratio vary throughout the optimization.

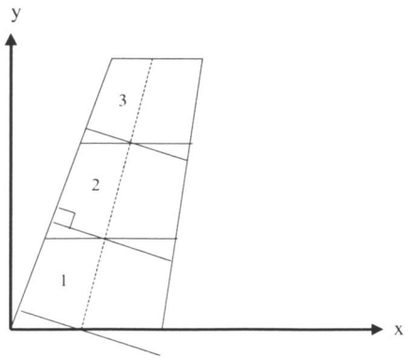

Figure 3. Wing Model

More detail of the wingbox model is shown in Figure 4. The thickness of sandwich face sheets, t, and the sandwich caliper thickness, t_s, are design variables in the top and bottom panels and in the webs of each bay. Stress and deformation analysis, and evaluation of the local buckling constraints, are kept at an elementary level commonly used in thin-walled structure applications (e.g., Bruhn, 1965). The Appendix contains a full development of this model and further explanation of Figure 4.

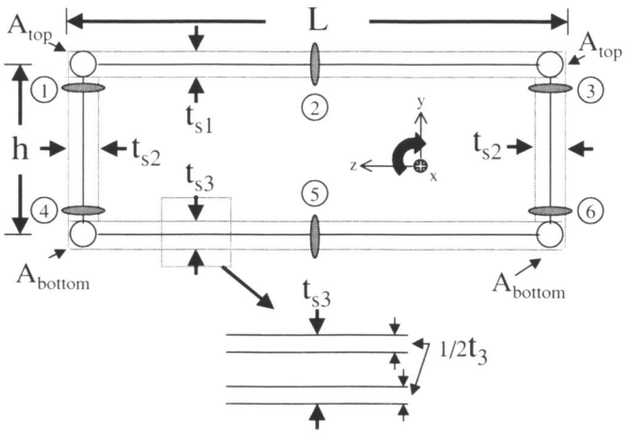

Figure 4. Wingbox Model

AERODYNAMICS – The aerodynamics module is constructed such that drag variations due to wing twist and weight, both input from the structures module, are effectively modeled. These variations must be continuously computed and updated in response to both design and behavior variable changes throughout the complete optimization process. To accomplish this, the aerodynamic analysis is broken down into its most fundamental equations, and lift and drag coefficients for both the wing and the horizontal tail are independently developed.

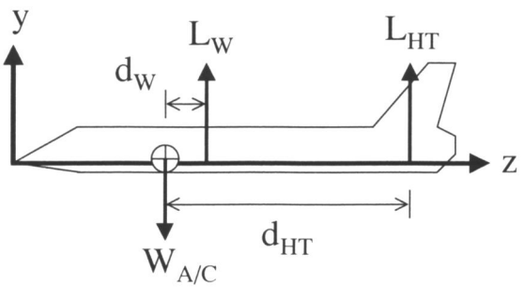

Figure 5. A/C Free Body Diagram

Beginning with the free body diagram in Figure 5, L_W and L_{HT} are the wing and horizontal tail lift, respectively, and d_W and d_{HT} are the corresponding distances from the aircraft center of gravity. $W_{A/C}$ is the weight of the aircraft. Summing forces in the y-direction

$$L_{W,0} + L_{HT,0} = W_{A/C} = L_{T,0}$$
$$\rightarrow C_{Lw,0} qS_{REF} + C_{Lht,0} \eta_H qS_{HT} = L_{T,0} \qquad (1)$$

where $L_{T,0}$ is the total lift produced by the aircraft. The $_0$ subscript indicates that the variable represents a value existing before the wing has been twisted (in following equations, subscript $_1$ denotes post wing twist values, before the aircraft is retrimmed).

In the same manner, sum the moments about the center of gravity to arrive at Equation 2.

$$L_{W,0} d_W + L_{HT,0} d_{HT} = M_{cg}$$
$$\rightarrow C_{Lw,0} \bar{d}_W + C_{Lht,0} \eta_H \frac{S_{HT}}{S_{REF}} \bar{d}_{HT} = 0 \qquad (2)$$

Here, the bar over each distance value indicates that it has been non-dimensionalized by the mean aerodynamic chord. In the above two equations, the unknown values $C_{Lw,0}$ and $C_{Lht,0}$ may be determined. $L_{w,1}$ is computed by subtracting lift lost to wing twist, calculated in the structures module, from the original lift, $L_{w,0}$. The corresponding lift coefficient is

$$C_{Lw,1} = \frac{L_{w,1}}{qS_{REF}} \qquad (3)$$

Summing the moments once more, this time using the post twist values, Equation 4 results,

$$C_{Lw,1} \bar{d}_W + C_{Lht,1} \eta_H \frac{S_H}{S_{REF}} \bar{d}_{HT} = 0 \qquad (4)$$

from which $C_{Lht,1}$ may be determined.

At this point, the forces and moments on an aircraft in level trimmed flight have been summed in Equations 1 and 2, without allowing the wings to twist. The rigid wing constraint was then dropped and the resulting change in wing lift, without retrimming the aircraft was used to determine $L_{w,1}$ in Equation 3. In order to retrim the aircraft and maintain the former flight path, lift on both the wing and horizontal tail must change accordingly. Speaking in terms of non-dimensional lift coefficients, $C_{Lw,1}$ and $C_{Lht,1}$ must be changed by ΔC_{Lw} and ΔC_{Lht}, which are essentially the differences between the "post" wing twist and "pre" wing twist coefficient values. A solution for trim drag is then approximated by

$$C_{D,trim} = k_w \Delta C_{Lw}^2 + k_{ht} \Delta C_{Lht}^2 \qquad (5)$$

where the right hand side is the drag from lift required to retrim the aircraft after wing twisting. Total drag is then calculated as

$$C_D = C_{D,\min} + C_{D,trim} + k_w C_{Lw,0}^2 + k_{ht} C_{Lht,0}^2 \qquad (6)$$

PROPULSION – To consider the requirement of having continuous functions for input and output into the optimization routine, the propulsion module is built around a surface fit to engine deck data for a double spool, mixed flow turbofan engine, designed for operation at high Mach numbers. Thrust is an independent variable and is allowed to range across all possible power settings for each respective altitude and Mach number combination. Accordingly, the second and third independent variables are altitude and Mach number with ranges between 30,000 to 60,000 feet and Mach 1.4 to 1.8, respectively. Experimentation indicated that between these limits the surface fit returns very accurate solutions with specific fuel consumption (SFC) as the dependent variable.

In order to allow an optimization routine control of thrust at the local level, a throttle setting variable was created by non-dimensionalizing net thrust available at each Mach number and altitude by the maximum net thrust available at those conditions. For instance, a throttle setting of 1 indicates maximum power at altitude and Mach number, while a throttle setting of 0.01 is idle thrust. Since maximum thrust available varies with altitude and Mach number as well, a second surface fit was constructed to represent this value, in order to non-dimensionalize the throttle setting variable.

While specific fuel consumption is an important output of the propulsion module, engine weight must also be calculated for input into the structures module. This is accomplished through the use of an engine scale factor (ESF)

$$ESF = \left(\frac{Gross\ Thrust}{Baseline\ Gross\ Thrust} \right)_{Sea\ Level} \qquad (7)$$

where the baseline gross thrust at sea level is provided with the engine data (reference AIAA..."Engine Data Package", 1995/1996). From this, the weight of the engine is

$$W_{ENG} = (Baseline\ Engine\ Weight)(ESF)^{1.05} \qquad (8)$$

To represent the effect of engine size on the aircraft's drag characteristics, engine scale factor is also input to the aerodynamics module where it is used to calculate a nacelle drag as part of $C_{D,min}$.

RANGE – Range calculation is performed in its own module through the Breguet range equation

$$R = \frac{V\left(L/D\right)}{SFC} \ln\left(\frac{W_T}{W_T - W_F} \right) \qquad (9)$$

where V is the velocity, a system level variable; L/D is the lift-to-drag ratio, output from the aerodynamics module; SFC is specific fuel consumption from the propulsion module; and W_T and W_F are the total aircraft weight and the weight of fuel burned, both output from the structures module.

The range module receives input from each of the subsystems at the local level and its output is treated as the objective function in the optimization method.

MODEL IMPLEMENTATION

As previously mentioned, variables in the BLISS method are organized as X, Y, or Z, depending on their location in the system structure. With the internal mechanisms of each subsystem defined, one must now determine the data flow such that it fits this organization.

Figure 6 shows the data dependencies for the business jet model as applied to the BLISS method and Table 1 is the corresponding variable definitions. As depicted, there are eight Z-variables in this model. Each of these design variables are shared by at least two subsystems and are therefore manipulated by the optimization method at the system level.

At the local level, the propulsion module has throttle setting as its only X-variable. The aerodynamics module contains the unique design variables of tail sweep and distances from the aircraft center of gravity to both the wing and tail aerodynamic centers. Note that if a stability and control module were included in this model, these latter two distances would be controlled at the system level, since they affect both aerodynamic and stability characteristics. Finally, the structures module is the most complex with nineteen local design variables. These include the wing taper ratio and the aluminum and monolithic plate thicknesses portrayed in Figure 4. Each thick-

ness array has nine elements: three thicknesses per wingbox bay multiplied by three bays per wing. The thicknesses are used in computing both wing weight and the stress values to be controlled as constraints in the local optimization.

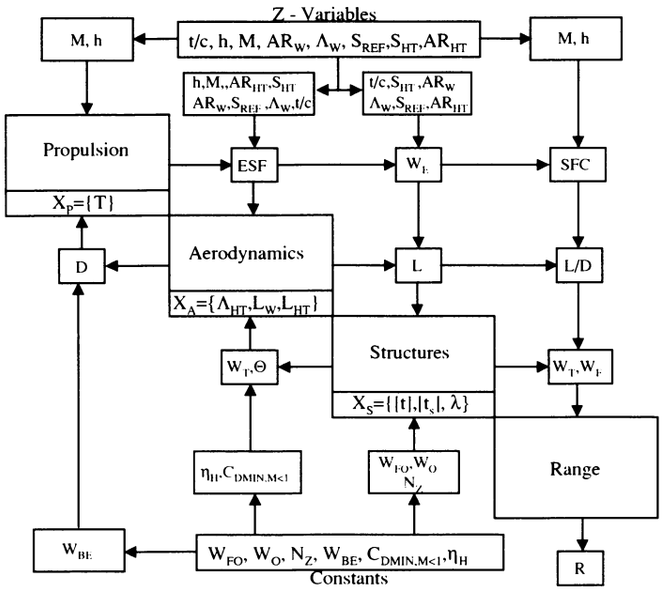

Figure 6. Data Dependencies for Business Jet Model

Table 1. Design and Behavior Variable Definitions

T-throttle	D-drag	AR$_W$- wing aspect ratio
Λ_{HT}- tail sweep	ESF-eng. scale fact.	AR$_{HT}$- tail aspect ratio
L$_W$-see Figure 1	L-lift	h-altitude
L$_{HT}$-see Figure 1	N$_Z$-max. load fact.	M-Mach #
|t|-thickness array, size 1x9	R-range	S$_{REF}$-wing surf. area
	SFC-spec. fuel cons.	S$_{HT}$-tail surf. area
|t$_S$|-thickness array, size 1x9	Θ-wing twist	t/c-thickness/chord
	W$_E$-engine weight	Λ_W-wing sweep
λ-taper ratio	W$_F$-fuel weight	
	W$_T$-total weight	
X	Y	Z

There are ten behavior, or Y-variables, that are not directly manipulated by the optimization routine. These are indicated in Figure 6 by arrows flowing from one module to another. Y-variables are calculated by means of a Gauss-Seidel iteration during the system analysis, prior to step 1 in Figure 2. At the beginning of each BLISS cycle, they are updated through this iteration, based on the updated values of X and Z from the previous optimization cycle.

Table 2. Side Constraints

constraint\variable	T	Λ_{HT} (deg)	L$_W$ (%MAC)	L$_{HT}$ (%MAC)	[t] (in)
lower	0.1	40	0.01	1.0	0.012
upper	1.0	70	0.2	3.5	0.9
constraint\variable	[t$_s$] (in)	λ_W	t/c	h (ft)	M
lower	0.012	0.1	0.01	30000	1.4
upper	18	0.4	0.09	60000	1.8
constraint\variable	AR$_W$	Λ_W (deg)	S$_{REF}$ (ft^2)	S$_{HT}$ (ft^2)	AR$_{HT}$
lower	2.5	40	200	50	2.5
upper	8.5	70	800	150	8.5

To avoid ill-conditioning of the optimization problem, i.e. ensure that the solution at the end of each BLISS cycle remains within a feasible design space, constraints must be formulated to control both the system and the local variables. The propulsion subsystem is governed by two constraints, one on the value of engine scale factor, ESF, and the other on the throttle setting. Engine scale factor boundaries are set to ensure that engine weight (eq. 8) and nacelle drag approximations remain accurate, while the throttle setting limitations ensure maximum thrust varies correctly with Mach number and altitude. A limit on pressure drag is the only constraint in the aerodynamics module. This is essentially constructed as a function of thickness-to-chord ratio to prevent unrealistic wing thicknesses for a high Mach number transport. There are forty-two constraints evaluated in the structures module. Thirty of these correspond to the stress calculations in Equations A6, A7, and A8 in the Appendix. The remaining twelve are restrictions on wingbox thicknesses that ensure physical dimensions remain realistic. For example, the thickness designated t_3 in Figure 4 must not be greater than t_{s3}. Finally, side constraints and move limits are placed on each of the X and Z design variables. Side constraints for the business jet model are in Table 2 and move limits are ± 20% of the variable's initial value.

In summary, twenty-three local level design variables, ten behavior variables, and eight system level variables characterize the business jet model. Forty-five constraints are in place while move limits and side constraints limit each of the design variables.

RESULTS

Application of the BLISS method to the business jet model was performed using MATLAB 5.3.0 software and its Optimization Toolbox. The same optimization routine was used independently on each of the four subsystems and at the system level. Convergence criteria for the system analysis iteration on behavior variables (prior to step 1 in Figure 2) was 0.1 percent, and termination criteria for the BLISS procedure was a range delta of less than 10 nautical miles between cycles. Under these requirements, the design model took five cycles to reach an optimized range. Results for the objective function and each of the design variables are listed in Table 3.

Table 3. Supersonic Business Jet Results

var\cycle*	1	2	3	4	5
Range (NM)	1361	1745	2133	2185	2189
t_1** (inner)	2.000	1.863	1.789	1.547	1.518
t_1 (middle)	2.000	0.515	0.708	0.777	0.838
t_1 (outer)	2.000	0.214	0.289	0.321	0.356
t_2 (inner)	2.000	0.315	0.460	0.347	0.343
t_2 (middle)	2.000	0.460	0.336	0.220	0.212
t_2 (outer)	2.000	0.155	0.129	0.088	0.085
t_3 (inner)	2.000	1.863	1.571	1.440	1.436
t_3 (middle)	2.000	0.477	0.595	0.692	0.770
t_3 (outer)	2.000	0.195	0.248	0.267	0.286
t_{s1} (inner)	4.000	1.863	1.887	1.971	1.980
t_{s1} (middle)	4.000	3.142	1.805	1.540	1.436
t_{s1} (outer)	4.000	1.777	0.996	0.833	0.754
t_{s2} (inner)	4.000	0.315	0.460	0.347	0.343
t_{s2} (middle)	4.000	0.460	0.336	0.220	0.212
t_{s2} (outer)	4.000	0.155	0.129	0.092	0.090
t_{s3} (inner)	4.000	1.863	2.020	2.054	2.044
t_{s3} (middle)	4.000	3.411	2.106	1.686	1.525
t_{s3} (outer)	4.000	1.967	1.154	0.984	0.904
λ_w	0.25	0.1	0.1	0.1	0.1
Λ_{HT} (°)	55	70	70	70	70
L_w (%MAC)	0.1	0.01	0.01	0.01	0.01
L_h (%MAC)	2.5	3.5	3.5	3.5	3.5
T	0.5000	0.1203	0.1562	0.1606	0.1607
t/c	0.050	0.075	0.083	0.083	0.083
h (ft)	50000	60000	59296	59296	59296
M	1.6	1.4	1.4	1.4	1.4
AR_w	5.50	7.57	6.91	6.91	6.91
Λ_w (°)	55	40	40	40	40
S_{REF} (ft^2)	500.0	361.7	434.4	434.4	434.4
S_{HT} (ft^2)	100.0	150.0	148.9	148.9	148.9
AR_{HT}	5.5	2.5	2.5	2.5	2.5

*One cycle is one pass through the BLISS procedure

**All thicknesses are in inches; inner, middle, outer refer to position along wing

Using wing and tail geometry from Table 3, Figure 7 displays the evolution of each lifting surface throughout the BLISS procedure. The horizontal tail reaches its final planform after the second cycle, while the wing passes through two iterations before converging in cycle 3. Since the stress constraints are highly sensitive to wing geometry, the reduction in wing sweep from 55 degrees to 40 degrees between the 1st cycle and the 2nd should be expected. Note that this occurred even though the derivative of the overall objective function with respect to wing sweep was not large (see Figure 10).

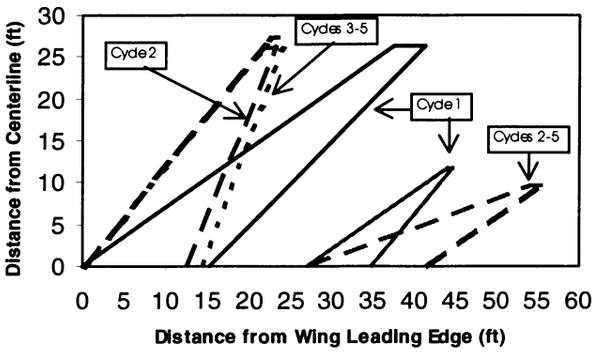

Figure 7. Wing and Tail Geometry

Observing the trend in wingbox thicknesses during the optimization procedure, t_3 and t_{s3} in Figure 4 are plotted accordingly in Figure 8. Initial thicknesses are 2 inches for t_3 and 4 inches for t_{s3} in all three wingbox bays along the half-span and the satisfaction of stress constraints, coupled with the optimization of range (reduction in weight), drives them to their final value in cycle 5.

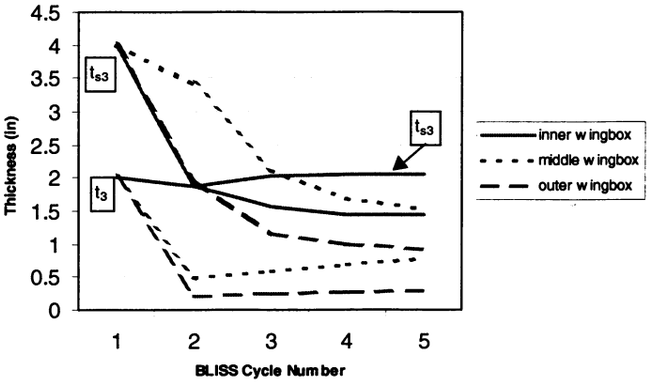

Figure 8. Thickness Plot of t_3 and t_{s3}

Larger stress values and an increased trim drag coefficient are a result of wing twist due to bending in a more highly swept wing. From Figure 9, note a similar trend to the wing geometry plot in Figure 7. Between cycles 1 and 2, a large reduction in wing twist corresponds to the large reduction in wing sweep. A reduction in trim drag by two orders of magnitude was also observed between cycles 1 and 2.

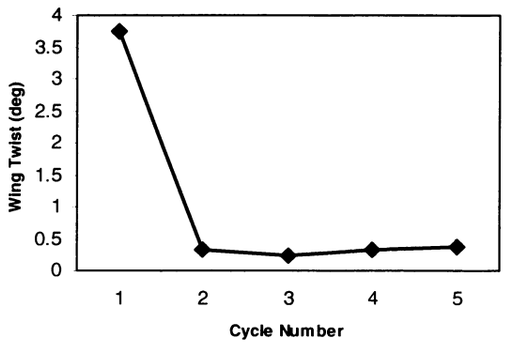

Figure 9. Wing Twist

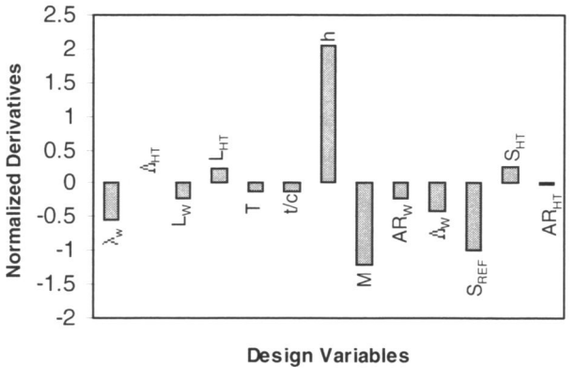

Figure 10. Range Sensitivities (1st cycle)

Finally, Figure 10 shows range sensitivities to both the X and Z variables. These values are literally the derivatives of the objective function, range, with respect to each of the design variables. As expected, variations in Mach number and altitude contribute the most to changes in range, while the horizontal tail sweep contributes the least.

CONCLUSION

A supersonic business jet design model was tailored for Bi-Level Integrated System Synthesis (BLISS), a Multidisciplinary Design Optimization method. Implementation included the division of the design model into four subsystems, each subject to autonomous local level optimizations linked to a system level optimization by optimum sensitivity data. Guided by implementation requirements of the BLISS method, particular emphasis was given to the proper representation of trade-offs and constraints influencing the design objective function. Additionally, continuous data flow within the above structure was ensured throughout model development, and the internal composition of each subsystem was represented by continuous functions. Results obtained through the use of MATLAB programming software indicated that an effective design model was developed and tailoring requirements were met.

REFERENCES

1. Balling, R. J.; and Sobieszczanski-Sobieski, J.: "Optimization of Coupled Systems: A Critical Overview of Approaches," AIAA J., Vol. 34, No. 1, pp. 6-17, Jan. 1996.
2. Bruhn, E. F.; "Analysis and Design of Flight Vehicle Structures", Tri-State Offset Co., Cincinnati, OH, Jan. 1996.
3. AIAA/UTC/Pratt & Whitney Undergraduate Individual Aircraft Design Competition, "Engine Data Package for the Supersonic Cruise Business Jet RFP." 1995/1996.
4. AIAA/UTC/Pratt & Whitney Undergraduate Individual Aircraft Design Competition, "Supersonic Cruise Business Jet RFP." 1995/1996.
5. MATLAB, the MathWorks, Inc., 1984-1999, version 5.3.0, 21 Jan 1999, and MATLAB Optimization Toolbox.
6. Raymer, Daniel P.: *Aircraft Design: A Conceptual Approach*, American Institute of Aeronautics and Astronautics, Inc. 1992.
7. Sobieszczanski-Sobieski, J.; Agte, J.; and Sandusky, R.: "Bi-Level Integrated System Synthesis (BLISS)." AIAA-98-4916.
8. Sobieszczanski-Sobieski, J.; and Haftka, R. T.: "Multidisciplinary Aerospace Design Optimization: Survey of Recent Developments." Structural Optimization, pp. 1-23, Vol. 14, No. 1, August 1997.

NOTATION

The following contains notation used in both the main text and the Appendix.

C_{Lht}: Horizontal tail lift coefficient.
C_{Lw}: Wing lift coefficient.
d_{HT}: Distance from tail aerodynamic center to aircraft c.g.
d_W: Distance from wing aerodynamic center to aircraft c.g.
h: Wingbox height.
k: Factor of Safety and Applied load coefficient.
k_{ht}: Horizontal tail induced drag coefficient.
k_w: Wing induced drag coefficient.
L: Wingbox length.
L_{HT}: Horizontal tail lift.
L_T: Total aircraft lift.
L_W: Wing lift.
q: Dynamic pressure.
t: Thickness of wingbox sandwich face sheets.
t_s: Wingbox sandwich caliper thickness.
V: Velocity.
$W_{A/C}$: Aircraft weight.
W_{BE}: Weight of the baseline engine.
W_{FO}: Weight of fuel other than in the wing.
W_O: Structural weight not included in wing or tail weight.
X variable: Local level design variable.
Y variable: Behavior variables passed between subsystems.
Z-variable: System level design variable.

ΔX_{OPT}: Optimum change in local level variables.
ΔZ_{OPT}: Optimum change in system level variables.
η_H: Horizontal tail dynamic pressure ratio.
σ: Normal stress.
τ: Shear stress.
ϕ_b: Wing twist due to bending of a swept wing.
ϕ_t: Wing twist due to torsion.

APPENDIX

This appendix describes the development of the wing model, including stress analysis and the approximation of aeroelastic effects. For the following, please refer to Figure 4 in the main text.

WINGBOX MODEL

In accordance with skin-stringer theory, areas across the length and height of the wingbox are represented at the corners by Equation A1, where i=1, 2, and 3 for the three wingboxes.

$$\frac{A_1(i) = A_2(i) = A_{top}(i) = (1/2)t_1(i)L(i) + (1/6)t_2(i)h(i)}{A_3(i) = A_4(i) = A_{bottom}(i) = (1/2)t_3(i)L(i) + (1/6)t_2(i)h(i)} \quad \text{(A1)}$$

The skin is composed of a light filler core sandwiched between two thicknesses of 2024 Aluminum Alloy. By using an equivalent moment of inertia about the z-axis based on both t_s and t, defined in Figure 4, this construction attempts to effectively model skin thickness and weight growth in response to buckling constraints.

The center of inertia along the y-axis is determined from

$$\bar{Y}(i) = \Sigma \frac{\bar{Y}_n(i)A_n(i)}{A_n(i)} \quad \text{(A2)}$$

and the moment of inertia about the z-axis from

$$I_{ZZ}(i) = \Sigma A(i)_n \bar{y}_n(i)^2 \quad \text{(A3)}$$

following the same index notation as Equation A1. Normal stresses are then calculated using Equations A4 and A5

$$\sigma_{1,3}(i) = \frac{-M_Z(i)(0.95h(i) - \bar{Y}(i))}{I_{ZZ}(i)},$$

$$\sigma_{4,6}(i) = \frac{-M_Z(i)(0.05h(i) - \bar{Y}(i))}{I_{ZZ}(i)} \quad \text{(A4)}$$

$$\sigma_2(i) = \frac{-M_Z(i)(h(i) - \bar{Y}(i))}{I_{ZZ}(i)}, \quad \sigma_5(i) = \frac{-M_Z(i)(-\bar{Y}(i))}{I_{ZZ}(i)} \quad \text{(A5)}$$

Note that numbered subscripts in these and following equations correspond to the circled numbers on Figure 4 and, when separated by commas, indicate that the equation holds for each of those points. For instance, Equation A4 includes the normal stresses for points 1, 3, 4, and 6. The circled numbers correspond to the six points at which constraints are evaluated on the wingbox model. These include normal stress constraints according to Equation A6,

$$k\sigma_{eq1-6}(i) \le \sigma_{A1-6}(i) \quad \text{(A6)}$$

where the allowable stress, σ_A, is 65 ksi and buckling constraints due to shear and normal stress are from Equations A7 and A8.

$$\frac{\sigma_{1,2,3}(i)}{\sigma_{cr1,2,3}(i)} + \left(\frac{\tau_{1,2,3}(i)}{\tau_{cr1,2,3}(i)}\right)^2 \le \frac{1}{k} \quad \text{(A7)}$$

$$\frac{\sigma_5(i)}{\sigma_{cr5}(i)} + \left(\frac{\tau_5(i)}{\tau_{cr5}(i)}\right)^2 \le \frac{1}{k} \quad \text{(A8)}$$

Here, k is equal to 1.5, a factor of safety, multiplied by 4.0, the maximum applied load, n_z (Raymer). Equivalent stress for constraint points one through six is

$$\sigma_{eq1-6}(i) = \sqrt{\sigma_{1-6}(i)^2 + 3\tau_{1-6}(i)^2} \quad \text{(A9)}$$

where

$$\tau_{1,3}(i) = \frac{q(i)}{t_2(i)} + \tau_{1,3}^T(i) \quad \text{(A10)}$$

$$\tau_{4,6}(i) = \frac{-q(i)}{t_2(i)} + \tau_{1,3}^T(i) \quad \text{(A11)}$$

$$\tau_{2,5}(i) = \frac{q(i)}{t_{1,3}(i)} \quad \text{(A12)}$$

and shear flow due to M_X is determined by

$$q(i) = \frac{M_X(i)}{2L(i)h(i)} \quad \text{(A13)}$$

The shears, τ_1^T and τ_3^T, in Equations A8 and A9 are calculated from

$$\tau_1^T(i) = \frac{T_1(i)}{ht_2(i)}, \quad \tau_3^T(i) = \frac{-T_3(i)}{ht_2(i)} \quad \text{(A14)}$$

where

$$T_1(i) = P(i)\frac{L(i) - a(i)}{L(i)}, \quad T_3(i) = P(i)\frac{a(i)}{L(i)} \quad \text{(A15)}$$

Here, *P* is the load and *a* is the distance back from the leading edge of the wingbox to the point at which *P* is applied, according to Figure A1.

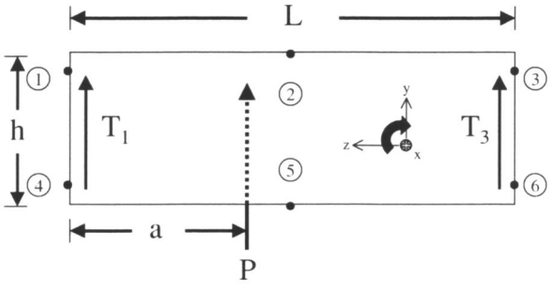

Figure A1.

Finally, the critical stresses, both normal and shear, found in Equations A7 and A8, come from the following equations. E is the modulus of elasticity, equal to 10,600 ksi for 2024 Aluminum Alloy, and ν is equal to 0.3.

$$\sigma_{cr1}(i) = \sigma_{cr3}(i) = \frac{\pi^2 E(4)}{12(1-\nu^2)}\left(\frac{t_{eq2}(i)}{0.95h(i)}\right)^2 \qquad \text{(A16)}$$

$$\sigma_{cr2,5}(i) = \frac{\pi^2 E(4)}{12(1-\nu^2)}\left(\frac{t_{eq1,3}(i)}{L(i)}\right)^2 \qquad \text{(A17)}$$

$$\tau_{cr1}(i) = \tau_{cr3}(i) = \frac{\pi^2 E(5.5)}{12(1-\nu^2)}\left(\frac{t_{eq2}(i)}{0.95h(i)}\right)^2 \qquad \text{(A18)}$$

$$\tau_{cr2,5}(i) = \frac{\pi^2 E(5.5)}{12(1-\nu^2)}\left(\frac{t_{eq1,3}(i)}{L(i)}\right)^2 \qquad \text{(A19)}$$

Equivalent thickness, denoted t_{eq} above, is obtained by representing a sandwich panel, shown in the cutout of Figure 4, by a monolithic plate of an equivalent cross sectional moment of inertia. Let this be I_S, based on t_s and t. Thus, the following derivation ensues, assuming unit width.

$$I(t_{eq}) = I_S \rightarrow \frac{(t_{eq})^3}{12} = \frac{(t/2)^3}{12}2 + \left(\frac{t}{2}\right)(2)\left(\frac{t_s - (t/2)}{2}\right)^2 \qquad \text{(A20)}$$

Solving for t_{eq}

$$t_{eq} = \left[\frac{t^3}{4} + 3t\left(t_s - \frac{t}{2}\right)^2\right]^{\frac{1}{3}} \qquad \text{(A21)}$$

AEROELASTIC EFFECTS

To effectively control aeroelastic characteristics of the wing model, twist due to both torsion and bending must be accounted for. Once thicknesses t_1, t_2, and t_3, are known along with the dimensions of the wing structural box, twist due to M_X can be calculated from Equation A22 for i=1, 2, and 3. G equals 4,000 ksi.

$$\phi_t(i) = \frac{M_X(i)}{4G(L(i)h(i))^2}\left(\frac{L(i)}{t_1(i)} + \frac{2h(i)}{t_2(i)} + \frac{L(i)}{t_3(i)}\right) \qquad \text{(A22)}$$

Determining wing twist due to the bending moment of a swept wing is accomplished by treating the displacements of a chord's leading and trailing edges as equivalent beam deflections.

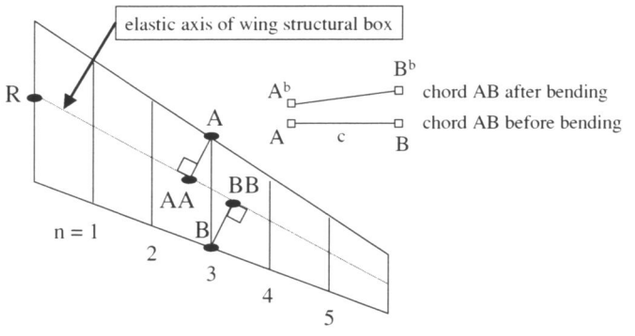

Figure A2. Twist due to Bending Model

Consider Figure A2, where the value of displacements ($A\text{-}A^b$) and ($B\text{-}B^b$) are desired. These deflections are proportional to the distances (R-AA) and (R-BB). More specifically, the deflection of point A is equivalent to the beam defection of point AA, and the deflection of B is equivalent to the beam deflection of BB. Due to the sweep of the wing, the distance (R-AA) is less than (R-BB) so that ($A\text{-}A^b$) < ($B\text{-}B^b$), and the steamline chord, n, rotates by

$$\phi_b = \frac{(B - B^b) - (A - A^b)}{c} \qquad \text{(A23)}$$

Total wing twist is then calculated as the sum of ϕ_b and ϕ_t.